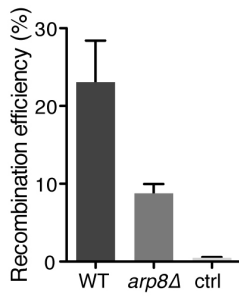
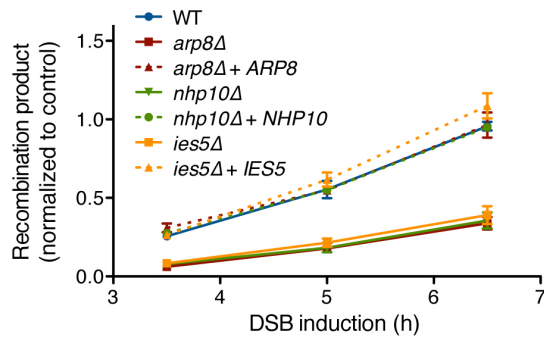
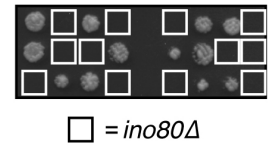
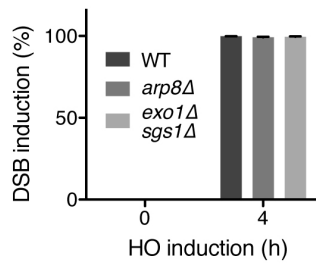
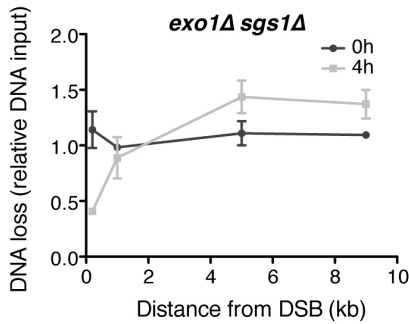
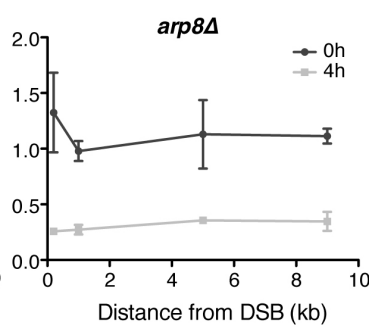
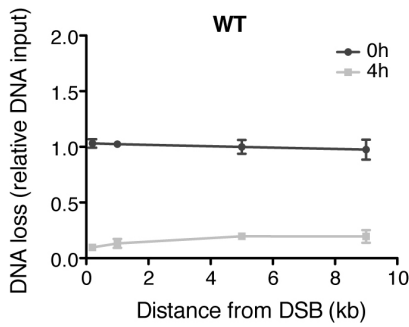
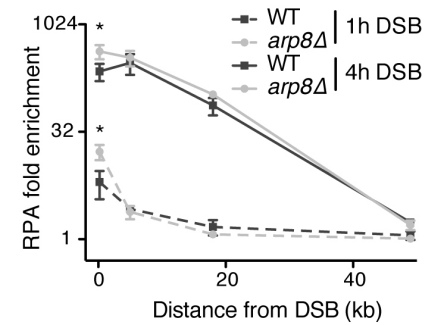
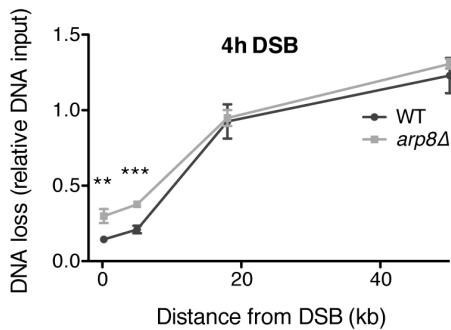
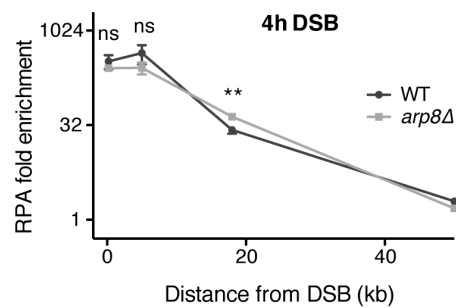


**Cell Reports, Volume 19**

**Supplemental Information**

**The INO80 Complex Removes H2A.Z  
to Promote Presynaptic Filament Formation  
during Homologous Recombination**

**Claudio A. Lademann, Jörg Renkawitz, Boris Pfander, and Stefan Jentsch**

**A****B****C****D****E****F****G**

**Figure S1; related to Figure 1.**

(A) *arp8Δ* cells are defective in HR. Survival assay following DSB induction at 491 kb on ChrIV. Only strains containing the donor sequence at 795 kb on ChrIV survive continuous expression of HO endonuclease to high rates. Ctrl: control strain without donor; n = 3 with error bars denoting SD.

(B) *ies5Δ* and *nhp10Δ* cells display a similar HR defect as *arp8Δ* cells. qPCR analysis of HR upon repair of a DSB at position 491 kb on ChrIV using a donor sequence at position 795 kb on ChrIV. Complementation of the respective knockout strains with an ectopically expressed version of the gene fully restores recombination; n = 3 with error bars denoting SD.

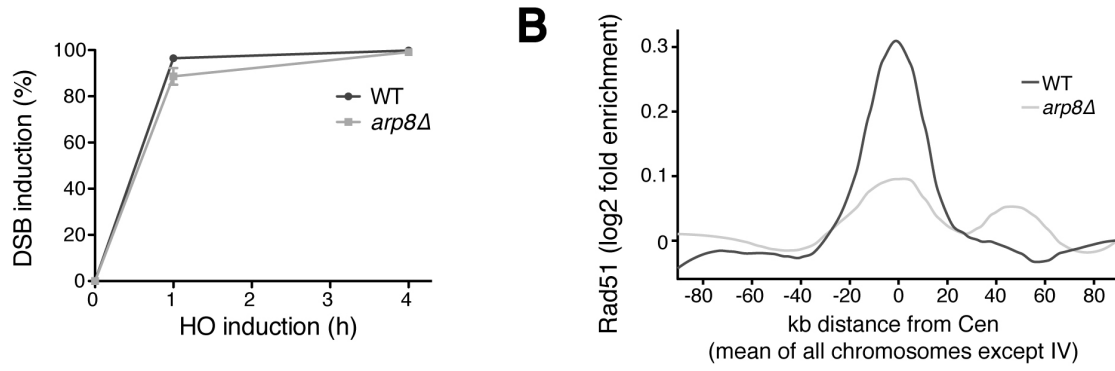
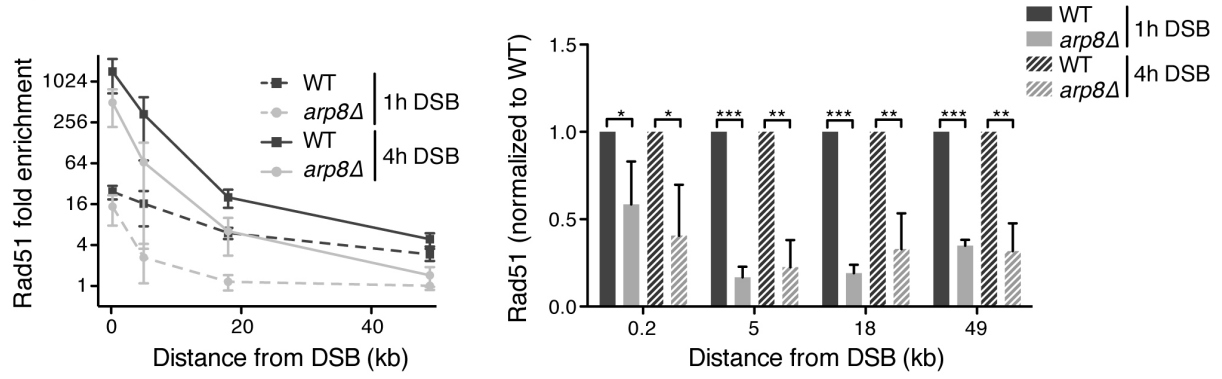
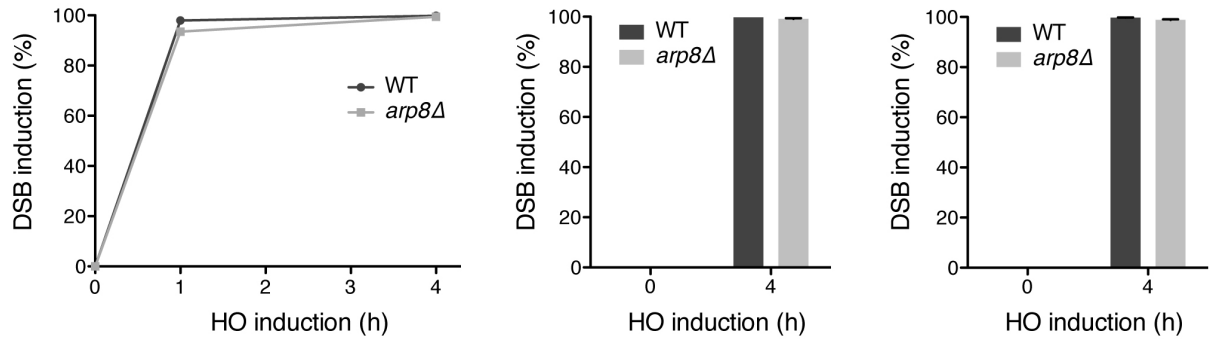
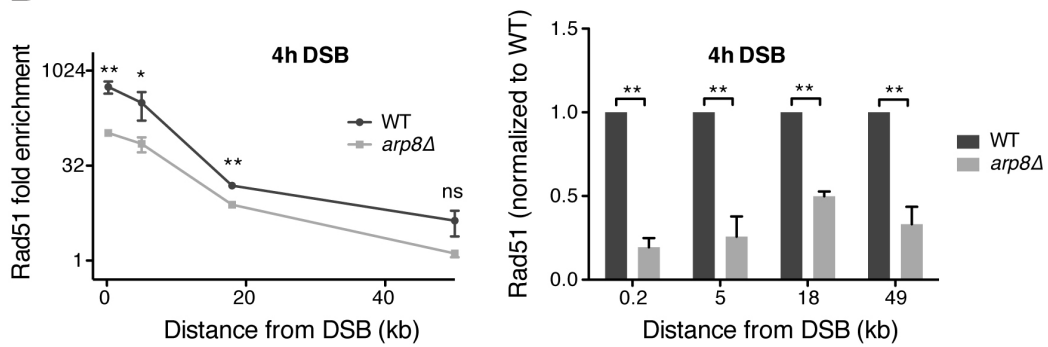
(C) Ino80 is essential in the W303 strain background. Tetrad analysis of diploid yeast cells each harboring heterozygous mutations (*ino80Δ::natNT2*, *htz1Δ::TRP1*, *GFPHOcs::hphNT1* and *GFPHOinc::kanMX4*). *ino80Δ* spores show poor viability.

(D) *arp8Δ* cells display reduced levels of DNA end resection. Upper panels and lower left panel: DNA loss analyzed by qPCR 4h following DSB induction at 491 kb on ChrIV. Lower right panel: DSB induction efficiency determined by qPCR using primers flanking the HO endonuclease recognition site. For all panels n = 3 with error bars denoting SD.

(E) *arp8Δ* cells display no defect in RPA accumulation at a DSB. Upper panel: ChIP against RPA analyzed by qPCR following DSB induction at 491 kb on ChrIV. Lower panel: DSB induction efficiency determined by qPCR using primers flanking the HO endonuclease recognition site. For both panels n = 3 with error bars denoting SD. \* p < 0.05.

(F) *arp8Δ* cells display reduced levels of DNA end resection. DNA loss analyzed by qPCR 4h following DSB induction at 166 kb on ChrVII; n = 3 with error bars denoting SD. \*\* p < 0.01 and \*\*\* p < 0.001.

(G) *arp8Δ* cells display no defect in RPA accumulation at a DSB. ChIP against RPA analyzed by qPCR following DSB induction at 166 kb on ChrVII; n = 3 with error bars denoting SD. \*\* p < 0.01 and ns not significant.

**A****C****D**

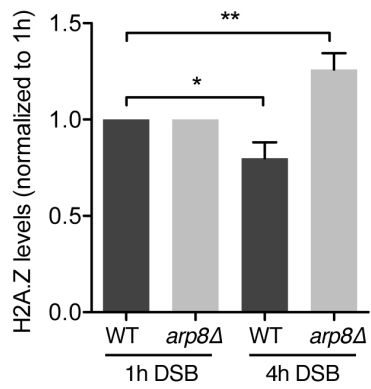
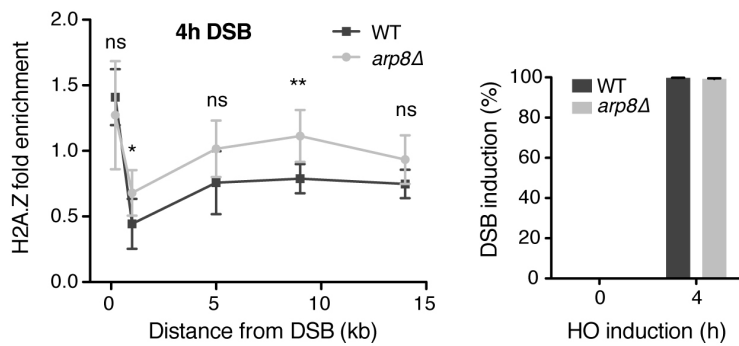
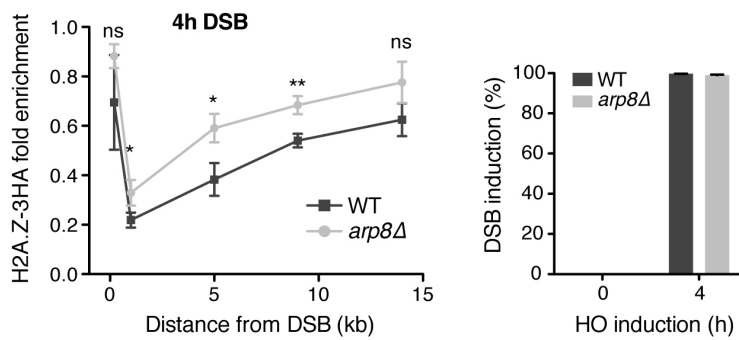
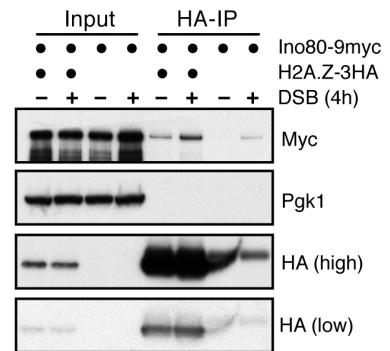
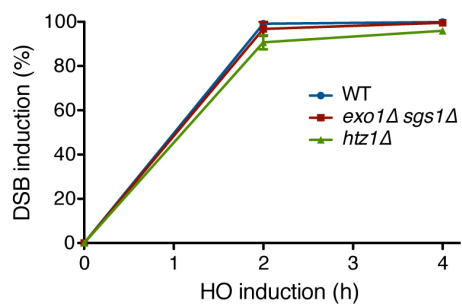
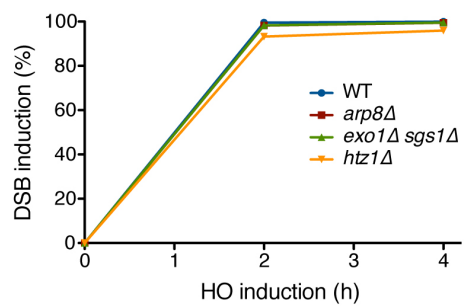
**Figure S2; related to Figure 2.**

(A) *arp8Δ* cells are defective in Rad51 filament formation. Left panel: ChIP against Rad51 analyzed by qPCR 1h or 4h after DSB induction at 491 kb on ChrIV. Right panel: Rad51 ChIP data as in left panel but normalized to the WT strain. Lower panel: DSB induction efficiency determined by qPCR using primers flanking the HO endonuclease recognition site. For all panels n = 4 with error bars denoting SD. \* p < 0.05, \*\* p < 0.01 and \*\*\* p < 0.001.

(B) *arp8Δ* cells are defective in inter-chromosomal homology search. Rad51 ChIP analyzed by deep sequencing (data from Figure 2A; n = 2). Depicted is the Rad51 fold enrichment around all centromeres except CenIV 4h following DSB induction. See supplemental experimental procedures for details on the analysis.

(C) DSB induction efficiency for experiments from Figure 2C (left panel), 2D (middle panel) and 2E (right panel) determined by qPCR using primers flanking the HO endonuclease recognition site. For all panels n = 3 with error bars denoting SD.

(D) *arp8Δ* cells are defective in Rad51 filament formation. Left panel: ChIP against Rad51 analyzed by qPCR 4h after DSB induction at 166 kb on ChrVII. Right panel: Rad51 ChIP data as in left panel but normalized to the WT strain. For both panels n = 3 with error bars denoting SD. \* p < 0.05, \*\* p < 0.01 and ns not significant.

**A****B****C****D****E****F**

**Figure S3; related to Figure 3.**

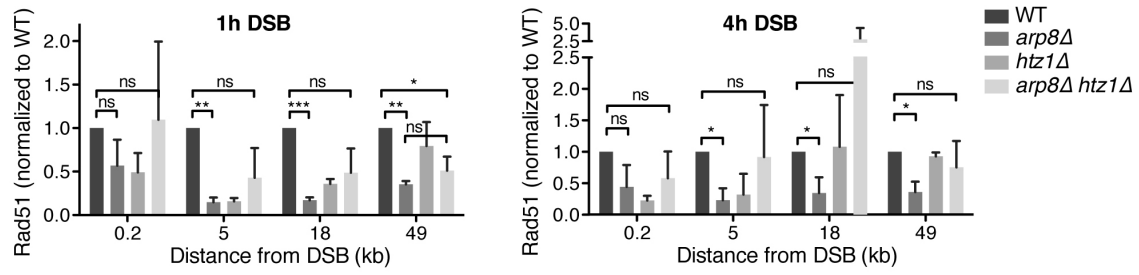
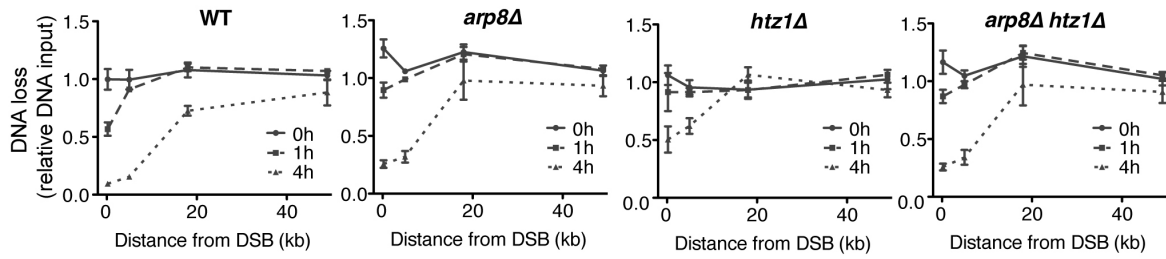
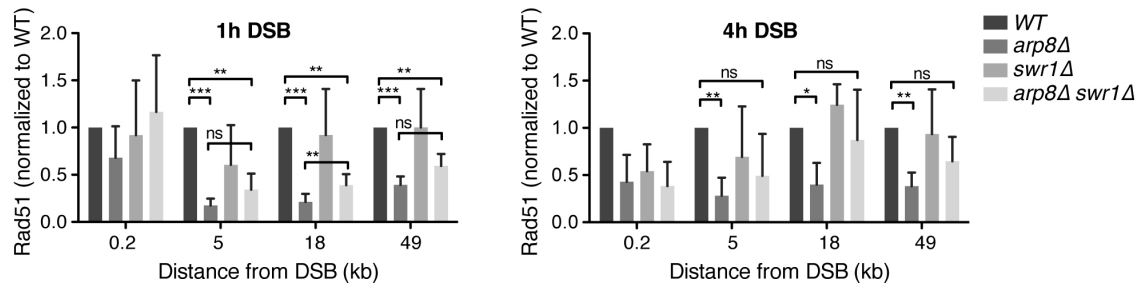
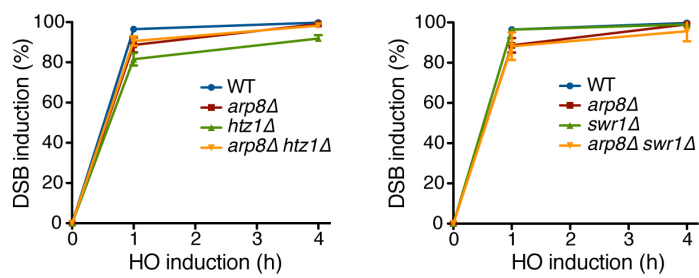
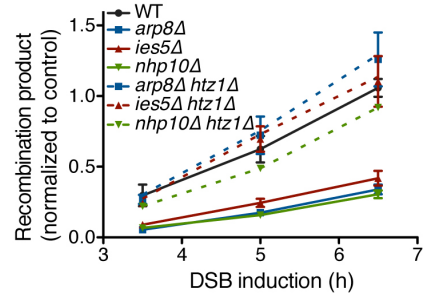
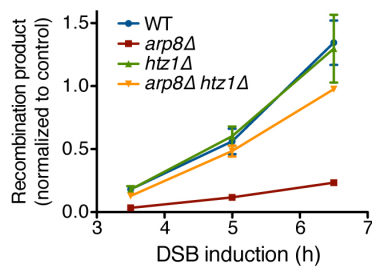
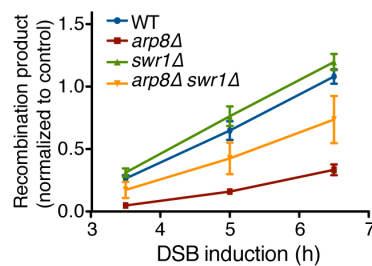
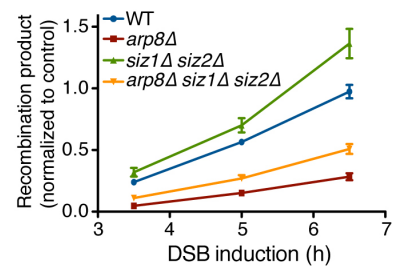
(A) H2A.Z is removed from DSBs over time in WT cells. H2A.Z ChIP signals from the experiment in Figure 3A quantified in an area comprising 5 kb on each side of the DSB and normalized to the 1h time point. Data represent the mean of all values derived from 500-bp window analysis (see supplemental experimental procedures) with error bars representing SEM. \*  $p < 0.05$  and \*\*  $p < 0.01$ .

(B) *arp8Δ* cells are defective in removing H2A.Z from DSB-adjacent chromatin. Left panel: ChIP against H2A.Z analyzed by qPCR following DSB induction at 491 kb on ChrIV. Right panel: DSB induction efficiency determined by qPCR using primers flanking the HO endonuclease recognition site. For both panels  $n = 6$  with error bars denoting SD. \*  $p < 0.05$ , \*\*  $p < 0.01$  and ns not significant.

(C) Left panel: ChIP against HA analyzed by qPCR indicating H2A.Z-3HA fold enrichment as analyzed in (A). Right panel: DSB induction efficiency determined by qPCR using primers flanking the HO endonuclease recognition site. For both panels  $n = 3$  with error bars denoting SD. \*  $p < 0.05$ , \*\*  $p < 0.01$  and ns not significant.

(D) INO80-C binding to H2A.Z is increased upon DSB induction. Immunoprecipitation of 3HA-tagged H2A.Z following DSB induction at 491 kb on ChrIV or in control cells and subsequent immunoblotting for the presence of 9Myc-tagged Ino80.

(E) and (F) DSB induction efficiencies for experiments in Figure 3D (E) and Figure 3E (F) determined by qPCR using primers flanking the HO endonuclease recognition site;  $n = 3$  with error bars denoting SD.

**A****B****C****D****E****F****G****H**

**Figure S4; related to Figure 4.**

(A) Removal of H2A.Z rescues Rad51 filament formation in the absence of Arp8. ChIP against Rad51 analyzed by qPCR following DSB induction at 491 kb on ChrIV and normalized to the WT strain; n = 3 with error bars denoting SD. \* p < 0.05, \*\* p < 0.01, \*\*\* p < 0.001 and ns not significant.

(B) Removal of H2A.Z does not rescue DNA end resection in the absence of Arp8. ChIP input DNA from experiment in (A) analyzed by qPCR following DSB induction at 491 kb on ChrIV; n = 3 with error bars denoting SD.

(C) Removal of Swr1 partially rescues Rad51 filament formation in the absence of Arp8. ChIP against Rad51 as indicated in (A); n = 3 with error bars denoting SD. \* p < 0.05, \*\* p < 0.01, \*\*\* p < 0.001 and ns not significant.

(D) DSB induction efficiencies for experiments in (A) and (B) (left panel) and (C) (right panel) determined by qPCR using primers flanking the HO endonuclease recognition site; n = 3 with error bars denoting SD.

(E) Removal of H2A.Z rescues HR in the absence of INO80-C subunits Ies5 and Nhp10. qPCR analysis of HR upon repair of a DSB at 491 kb on ChrIV using a donor sequence at 795 kb on ChrIV; n = 3 with error bars denoting SD.

(F) Removal of H2A.Z rescues HR in the absence of Arp8. qPCR analysis of HR upon repair of a DSB at 166 kb on ChrVII using a donor sequence at 434 kb on ChrVII; n = 3 with error bars denoting SD.

(G) Removal of Swr1 partially rescues HR in the absence of Arp8. qPCR analysis of a HR as indicated in (E).

(H) Removal of Siz1 and Siz2 partially rescues HR in the absence of Arp8. qPCR analysis of HR as indicated in (E).

## Supplemental Experimental Procedures

### Yeast strains and techniques

Yeast strains are listed in table “Yeast strains”. All strains are isogenic to W303. Strain YCL026 was obtained by crossing W303 *MATa* with YCZ173 (Zierhut and Diffley, 2008). Knockouts and chromosomally tagged strains were constructed usually in haploids by a PCR-based strategy (Janke et al., 2004; Knop et al., 1999). In case of strains YCL344, 345, 463, 661, 663, 682, 683, 692 and 793 deletions have been made in haploids of different mating types and final strains have been obtained by tetrad dissection of respective diploids. Deletions of *IES5* (strains YCL626 and 627) and *NHP10* (strains YCL734 and 735) have been generated directly in diploids with final strains obtained by subsequent tetrad dissections. In general, selection cassettes containing different marker genes (*kanMX4/6*, *hphNT1*, *natNT2*, *CaURA3*, *TRP1*) were amplified using gene specific overhangs, leading to their integration at the endogenous locus, thereby replacing the original gene. Correct cassette integration was determined by yeast colony PCR and chromosomal taggings were additionally confirmed by immunoblotting. For construction of yeast strains harboring site-specific *HO<sub>cs</sub>* or *GFP-HO<sub>cs</sub>* (sequence “H” in the recombination assay scheme in Fig. 1A), a 36-bp HO endonuclease recognition sequence (5'-AGTTTCAGCTTTCCGCAACAGTATAATTTTATAAAC-3') (Paques and Haber, 1997) was cloned via oligonucleotide annealing next to a marker gene in the pFA6a backbone or inside the GFP ORF of pYM25 (Janke et al., 2004), respectively, and this construct used for PCR amplification with site-specific overhangs for the destined integration site (ChrIV 491 kb, in-between *YDR024W* and *YDR025W*). In case of *GFP-HO<sub>inc</sub>* (sequence “HU” in the recombination assay scheme in Fig. 1A), a similar approach was undertaken, but with a mutated HO endonuclease recognition site (5'-AGTTTCAGCTTTCCaCAAtAGTATAATTTTATAAAC-3', mutations in lowercase) (Nickoloff et al., 1990) flanked by a unique 23-bp sequence (5'-CTAGCTGACGAAATGGCAAACAA-3') cloned into the GFP-encoding sequence of pYM12 (Knop et al., 1999). Integration was targeted at ChrIV 795 kb in between *YDR169C-A* and *YDR170C*. For recombination determination on ChrVII, a slightly modified system was used, comprising *GFP-HO<sub>cs2</sub>* (in which the GFP sequence was flanked 5' by a unique 90-bp sequence (5'-TGAAGAGATACGCCCTGGTTCCTATCCGGAAGCGACCAACGCCTTGATTGACAAGGATGGATGGC TACATTCTGGAGACATAGCTTACTG-3')) and *GFP-HO<sub>inc2</sub>* (harboring a different unique 23-bp sequence (5'-GGAAAACGCTGGGCGTAAATCAG-3') next to the mutated HO endonuclease recognition site). Integration was targeted at ChrVII 166 kb in between *YGL179C* and *YGL178W* and at ChrVII 434 kb in between *YGL035C* and *YGL033W*, respectively.

### Yeast strains

Strain	Genotype	Source
JOR097	YCL26, <i>ChrIV<sub>491kb</sub>::HOcs-hphNT1</i>	(Renkawitz et al., 2013)
YCL026	<i>MATa</i> , <i>ade3::P<sub>GAL</sub>-HO</i> , <i>hmlA::pRS-1 hmrΔ::pRS-2</i> <i>matHOcsΔ::pBR-1</i>	(Renkawitz et al., 2013)
YCL063	YCL26, <i>ChrIV<sub>491kb</sub>::GFPHOcs-hphNT1</i>	This study
YCL076	YCL63, <i>ChrIV<sub>795kb</sub>::GFPHOinc-kanMX4</i>	This study
YCL110	JOR97, <i>arp8Δ::kanMX6</i>	This study
YCL115	YCL76, <i>arp8Δ::natNT2</i>	This study
YCL179	JOR97, <i>sgs1Δ::kanMX6</i> , <i>exo1Δ::natNT2</i>	This study
YCL248	JOR97, <i>htz1Δ::natNT2</i>	This study
YCL252	JOR97, <i>swr1Δ::natNT2</i>	This study
YCL260	JOR97, <i>arp8Δ::kanMX6</i> , <i>swr1Δ::natNT2</i>	This study
YCL261	JOR97, <i>arp8Δ::kanMX6</i> , <i>htz1Δ::natNT2</i>	This study
YCL344	YCL76, <i>arp8Δ::natNT2</i> , <i>htz1Δ::CaURA3</i>	This study
YCL345	YCL76, <i>arp8Δ::natNT2</i> , <i>swr1Δ::CaURA3</i>	This study
YCL451	YCL76, <i>htz1Δ::natNT2</i>	This study
YCL463	YCL76, <i>arp8Δ::natNT2</i> , <i>siz1Δ::TRP1</i> , <i>siz2Δ::CaURA3</i>	This study
YCL513	JOR97, <i>RAD55-6HA::natNT2</i>	This study
YCL514	YCL110, <i>RAD55-6HA::natNT2</i>	This study

YCL515	JOR97, <i>RAD57-6HA::natNT2</i>	This study
YCL517	YCL110, <i>RAD57-6HA::natNT2</i>	This study
YCL537	YCL76, <i>swr1Δ::natNT2</i>	This study
YCL584	JOR97, <i>H2A.Z-3HA::TRP1</i>	This study
YCL587	JOR97, <i>H2A.Z-3HA::TRP1, INO80-9myc::natNT2</i>	This study
YCL588	YCL110, <i>H2A.Z-3HA::TRP1</i>	This study
YCL601	JOR97, <i>INO80-9myc::natNT2</i>	This study
YCL626	YCL76, <i>ies5Δ::natNT2</i>	This study
YCL627	YCL76, <i>ies5Δ::natNT2, htz1Δ::TRP1</i>	This study
YCL661	YCL76, <i>slx8Δ::CaURA3</i>	This study
YCL663	YCL76, <i>arp8Δ::natNT2, slx8Δ::CaURA3</i>	This study
YCL682	YCL76, <i>H2A.Z<sup>K126,133R</sup>-3HA::TRP1</i>	This study
YCL683	YCL76, <i>arp8Δ::natNT2, H2A.Z<sup>K126,133R</sup>-3HA::TRP1</i>	This study
YCL692	YCL76, <i>siz1Δ::TRP1, siz2Δ::CaURA3</i>	This study
YCL734	YCL76, <i>nhp10Δ::natNT2</i>	This study
YCL735	YCL76, <i>nhp10Δ::natNT2, Δhtz1::TRP1</i>	This study
YCL782	YCM26, <i>arp8Δ::natNT2</i>	This study
YCL792	YCM26, <i>htz1Δ::TRP1</i>	This study
YCL793	YCM26, <i>arp8Δ::natNT2, htz1Δ::TRP1</i>	This study
YCL806	YCL26, <i>ChrVII<sub>166kb</sub>::HOcs-hphNT1</i>	This study
YCL810	YCL806, <i>arp8Δ::kanMX6</i>	This study
YCL822	YCL115, <i>ARP8::LEU2</i>	This study
YCL823	YCL734, <i>NHP10::LEU2</i>	This study
YCL824	YCL626, <i>IES5::LEU2</i>	This study
YCM026	YCL26, <i>ChrVII<sub>166kb</sub>::GFPHOcs2-hphNT1, ChrVII<sub>434kb</sub>::GFPHOinc2-kanMX4</i>	This study

### Induction of single DSBs in vivo

DSB induction was performed as described (Kalocsay et al., 2009; Renkawitz et al., 2013). Briefly, yeast strains expressing the HO endonuclease gene under control of the GAL promoter were grown in YP-lactate medium (1% Bacto Yeast Extract, 2% Bacto Peptone, 3% lactic acid, pH 5.5) to avoid repressive effects of glucose on GAL promoter-driven expression. HO expression was typically induced at mid-log phase (OD<sub>600</sub> 0.5-0.8) by the addition of galactose to the lactate medium at a final concentration of 2% (w/v).

### Recombination survival assay

To measure recombination via cell survival, strains were streaked directly from glycerol stocks onto YP-Raffinose plates. After 3 days at 30°C, cells were serially diluted in PBS to an OD<sub>600</sub> of 10<sup>-5</sup> and 100 μl or 200 μl of this dilution were subsequently plated onto YPD or YP-GAL plates, respectively. After a sufficient growth time (2-4 days), single colonies were counted and the ratio between YP-GAL and YPD taken as recombination efficiency.

### ChIP and qPCR analysis

ChIP experiments were performed as described (Kalocsay et al., 2009; Renkawitz et al., 2013). Briefly, at each time point following DSB induction, 200 ml cultures were cross-linked by adding 1% (final concentration) formaldehyde for a total of 16 min. The reaction was stopped by addition of 375 mM (final concentration) glycine for a minimum of 10 min. Equal amounts of cells (usually 140 OD<sub>600</sub>) were then lysed using Silica beads and a multi-tube bead-beater (MM301, Retsch GmbH), the chromatin enriched by centrifugation and sheared to an average size of 300 bp by sonication (using a Bioruptor UCD-200, Diagenode). For immunoprecipitation, Protein A sepharose was combined with the following antibodies: anti-Arp5 (abcam,

ab12099), anti-H2B (Active Motif, 39237), anti-HA (abcam, ab9110), anti-H2A.Z (Active Motif, 39647), anti-Rad51 (SantaCruz, y-180; lot numbers: K1209 and C3007), anti-Rad52 (Sacher et al., 2006) and anti-RPA (Agrisera, AS07214). ChIP experiments were analyzed by qPCR using a Light Cycler LC480 system (Roche). Oligonucleotides used for qPCR are depicted in Table “Oligonucleotides”.

### Oligonucleotides

Sequence	Genomic Position
CAATGGACGAGGAAACAAGAGCGATT	ChrIV_509kb_fwd
ACCATAACCAGACCTTTTCCAGTCTGT	ChrIV_509kb_rev
AACCTGATTCTTATACAAGCAGCCAA	ChrIV_795kb_fwd
AATTGGAATGCCCCAGATTCTCAAAC	ChrIV_795kb_rev
ATTCCAGGCCAACCCAAGTAAGTC	ChrIV_491kb_fwd
CTTCTAGGAGGAGGAAAGCCCAT	ChrIV_491kb_rev
TGGGATAATGGTAGTACTGGGCGT	ChrIV_500kb_fwd
CAGCTGCTCCGAAACCAATTTTGA	ChrIV_500kb_rev
GTATACCTGACGGGCAGTCCTTTT	ChrIV_505kb_fwd
GCAGTGACGGTTCAAGATCTCCTT	ChrIV_505kb_rev
TACACATAAGAGGCTCATTAGGGC	ChrIV_540kb_fwd
CCAGCGTAATTATAGGATTGCCA	ChrIV_540kb_rev
GTTTCCCCAGCTTTCCTGT	ChrIV_492kb_fwd
TTGCTTCTGCAGAAGTGGAGA	ChrIV_492kb_rev
AGGGCCAACACCTAGTCCAA	ChrIV_496kb_fwd
AGGCGAAGTTAGTGCTGAACA	ChrIV_496kb_rev
TTCTTTCGCCAGGTGTTTTACCCA	ChrVII_166kb_fwd
AGGCCACGTTTAAAGAATGGCAAGA	ChrVII_166kb_rev
GCAATGACGTCCTACTAAAGTCCCA	ChrVII_171kb_fwd
TTTGGTAGGGAGCAATGCTAACCC	ChrVII_171kb_rev
AAACAAACGTGCGTATGCAAGACA	ChrVII_184kb_fwd
GCAGCAATGACAAAGTCGTTTGGA	ChrVII_184kb_rev
GGTCTTACACCTGCCACCTTTGAA	ChrVII_216kb_fwd
CGGGCGCTTATAAAACCGCTATG	ChrVII_216kb_rev
GCGTGCCTGGTCACAGGTTTCATACGAC	ChrX_MDV1_fwd
TCATACGGCCCAAATATTTACGTCCC	ChrX_MDV1_rev

### DSB induction efficiency

To determine DSB induction efficiency, ChIP input DNA was analyzed by qPCR using primers binding to sequences flanking the DSB, which were 5'-CATACTGTCTCACTCGCTTGG-3' upstream of the HO recognition site on ChrIV and 5'-GACTGTCAAGGAGGGTATTCTG-3' downstream of the HO recognition site as part of the *hphNT1* resistance cassette.

### Deep sequencing

For deep sequencing analysis, sequencing libraries of ChIP and input DNA were generated using the MicroPlex library preparation kit v2 including 48 indices (Diagenode) as described by the manufacturer's instructions. Sequencing of 50-bp single-end reads on an Illumina HiSeq 1500 sequencer at an average of 3 million reads per sample was performed by the Laboratory for Functional Genome Analysis (LAFUGA) at LMU Munich. ChIP-seq experiments were performed in duplicates and all samples in one experiment were sequenced together on a single lane using barcode multiplexing.

### Bioinformatic analysis of deep sequencing data

Raw data quality was analyzed using the FastQC tool (<http://www.bioinformatics.babraham.ac.uk/projects/fastqc/>) and data further processed using the R software

tool. Briefly, the fastq raw files were mapped to the *S. cerevisiae* genome (genome built R-64-1-1) using the bowtie1 aligner with standard parameters except  $-m=1$ . The genome was split into non-overlapping windows with a size of 500 bp and all successfully mapped reads assigned to their corresponding window(s) using the GenomicRanges R package (Lawrence et al., 2013). For a statistical comparison of input with IP samples the window counts were TMM-normalized (Robinson and Oshlack, 2010), the dispersion was estimated (Chen et al., 2014) and a negative binomial generalized log-linear model was fitted using a generalized linear model (McCarthy et al., 2012) using the edgeR (Robinson et al., 2010) R package. Normalized IP/input values were then written to wig files for visualization using publicly available genome browsers. For centromere-centered Rad51 analysis in Fig. S2C, BEDtools (Quinlan and Hall, 2010) was used to generate a saf file containing 500-bp windows of the regions surrounding all centromeres  $\pm 90$  kb, except CenIV. Reads in the respective windows were then counted from the mapped files using featureCounts (Liao et al., 2014) and the subsequently calculated normalized IP/input ratios of corresponding windows with similar linear distances averaged over all chromosomes. The ratios were plotted as a locally weighted regression using the geom\_smooth function of the ggplot2 R package (Wickham, 2009).

All data depicted present log<sub>2</sub> enrichments and were normalized to the corresponding 0 h time point.

### **Analysis of DNA end resection**

For determining the physical loss of DNA at DSBs, input DNA from ChIP experiments was analyzed by qPCR and values normalized to a control locus on chromosome X (*MDVI*). In case of samples derived from deep sequencing, raw data files from input sequencing libraries were processed as described above, including normalization to the uninduced state.

### **Co-immunoprecipitation analysis**

For protein-protein interaction studies involving co-IP, native yeast extracts were prepared by cell disruption using Silica beads and a multi-tube bead-beater (MM301, Retsch GmbH) in IP lysis buffer (50 mM Tris HCl pH7.5, 150 mM NaCl, 10% (v/v) glycerol, 2 mM MgCl<sub>2</sub>, 0.5% (v/v) NP-40). To avoid protein degradation, lysis buffer was freshly supplemented with protease inhibitors. Chromatin interactions were enriched by sonication for 10 min using the Bioruptor UCD-200 sonication system (Diagenode) and cell debris removed by centrifugation. Immunoprecipitation was conducted for 3 h at 4°C on a rotating wheel using an anti-HA affinity matrix (Roche Diagnostics GmbH) followed by three washing steps in IP lysis buffer to remove non-specific background binding to the beads. Immunoprecipitated material was analyzed by standard immunoblot analysis.

### **Chromatin binding assay**

To analyze histone removal from chromatin, cells were G2/M arrested using nocodazole and subsequently subjected to DNA damage by phleomycin. Immediately after harvesting, ATP-dependent processes were blocked by addition of sodium azide and sodium fluoride until all samples were collected. Spheroblasts were then prepared by cell wall digestion and lysed using detergent containing buffer (50 mM KAc, 2 mM MgCl<sub>2</sub>, 20 mM Hepes pH 7.9, 0.5% Triton X-100). Chromatin and soluble fraction were separated on a sucrose cushion (50 mM Hepes pH7.5, 100 mM KCl, 2.5 mM MgCl<sub>2</sub>, 0.4 M Sorbitol, 1 mM DTT, 0.25% Triton X-100, 30% Sucrose), protein extracts prepared by TCA precipitation and analyzed by standard immunoblot analysis. To avoid protein degradation, all buffers were freshly supplemented with protease inhibitors.

## Supplemental References

- Chen, Y., Lun, A., Smyth, G.K., 2014. Differential expression analysis of complex RNA-seq experiments using edgeR. ... analysis of next generation sequencing data. doi:10.1007/978-3-319-07212-8\_3
- Janke, C., Magiera, M.M., Rathfelder, N., Taxis, C., Reber, S., Maekawa, H., Moreno-Borchart, A., Doenges, G., Schwob, E., Schiebel, E., Knop, M., 2004. A versatile toolbox for PCR-based tagging of yeast genes: new fluorescent proteins, more markers and promoter substitution cassettes. *Yeast* 21, 947–962. doi:10.1002/yea.1142
- Knop, M., Siegers, K., Pereira, G., Zachariae, W., Winsor, B., Nasmyth, K., Schiebel, E., 1999. Epitope tagging of yeast genes using a PCR-based strategy: more tags and improved practical routines. *Yeast* 15, 963–972. doi:10.1002/(SICI)1097-0061(199907)15:10B<963::AID-YEA399>3.0.CO;2-W
- Lawrence, M., Huber, W., Pagès, H., Aboyoun, P., Carlson, M., Gentleman, R., Morgan, M.T., Carey, V.J., 2013. Software for computing and annotating genomic ranges. *PLoS Comput. Biol.* 9, e1003118. doi:10.1371/journal.pcbi.1003118
- Liao, Y., Smyth, G.K., Shi, W., 2014. featureCounts: an efficient general purpose program for assigning sequence reads to genomic features. *Bioinformatics* 30, 923–930. doi:10.1093/bioinformatics/btt656
- McCarthy, D.J., Chen, Y., Smyth, G.K., 2012. Differential expression analysis of multifactor RNA-Seq experiments with respect to biological variation. *Nucleic Acids Res.* 40, 4288–4297. doi:10.1093/nar/gks042
- Nickoloff, J.A., Singer, J.D., Heffron, F., 1990. In vivo analysis of the *Saccharomyces cerevisiae* HO nuclease recognition site by site-directed mutagenesis. *Mol. Cell. Biol.* 10, 1174–1179.
- Paques, F., Haber, J.E., 1997. Two pathways for removal of nonhomologous DNA ends during double-strand break repair in *Saccharomyces cerevisiae*. *Mol. Cell. Biol.* 17, 6765–6771. doi:10.1128/MCB.17.11.6765
- Quinlan, A.R., Hall, I.M., 2010. BEDTools: a flexible suite of utilities for comparing genomic features. *Bioinformatics* 26, 841–842. doi:10.1093/bioinformatics/btq033
- Robinson, M.D., McCarthy, D.J., Smyth, G.K., 2010. edgeR: a Bioconductor package for differential expression analysis of digital gene expression data. *Bioinformatics* 26, 139–140. doi:10.1093/bioinformatics/btp616
- Robinson, M.D., Oshlack, A., 2010. A scaling normalization method for differential expression analysis of RNA-seq data. *Genome Biol.* 11, R25. doi:10.1186/gb-2010-11-3-r25
- Sacher, M., Pfander, B., Hoegge, C., Jentsch, S., 2006. Control of Rad52 recombination activity by double-strand break-induced SUMO modification. *Nat Cell Biol* 8, 1284–1290. doi:10.1038/ncb1488
- Wickham, H., 2009. ggplot2: elegant graphics for data analysis.
- Zierhut, C., Diffley, J.F.X., 2008. Break dosage, cell cycle stage and DNA replication influence DNA double strand break response. *EMBO J* 27, 1875–1885. doi:10.1038/emboj.2008.111